






## Optical detection of the susceptibility tensor in two-dimensional crystals

Zhemi Xu<sup>1,2</sup>, Davide Ferraro<sup>1</sup>, Annamaria Zaltron<sup>1</sup>, Nicola Galvanetto<sup>1</sup>, Alessandro Martucci <sup>3</sup>, Luzhao Sun <sup>4,5</sup>, Pengfei Yang<sup>6</sup>, Yanfeng Zhang <sup>6</sup>, Yuechen Wang<sup>4,5</sup>, Zhongfan Liu <sup>4,5</sup>, Joshua D. Elliott<sup>7</sup>, Margherita Marsili<sup>1</sup>, Luca Dell'Anna <sup>1</sup>, Paolo Umari<sup>1</sup> & Michele Merano<sup>1</sup>✉

The out-of-plane optical constants of monolayer two-dimensional materials have proven to be experimentally elusive. Owing to their reduced dimensionality, optical measurements have limited sensitivity to these properties which are hidden by the optical response of the substrate. Therefore, there remains an absence of scientific consensus on how to correctly model these crystals. Here we perform an experiment on the optical response of a single-layer two-dimensional crystal that addresses these problems. We successfully remove the substrate contribution to its optical response by a step deposition of a monolayer crystal inside a thick polydimethylsiloxane prism. This allows for a reliable determination of both the in-plane and the out-of-plane components of its surface susceptibility tensor. Our results prescribe one clear theoretical model for these crystals. This precise characterization of their optical properties will be relevant to future progresses in photonics and optoelectronics with two-dimensional materials.

<sup>1</sup>Dipartimento di Fisica e Astronomia “Galileo Galilei”, Università degli Studi di Padova, via Marzolo 8, I-35131 Padova, Italy. <sup>2</sup>College of Chemistry and Materials Engineering, Beijing Technology and Business University, Beijing 100048, PR China. <sup>3</sup>Dipartimento di Ingegneria Industriale, Università degli Studi di Padova, via Marzolo 9, I-35131 Padova, Italy. <sup>4</sup>Center for Nanochemistry, Beijing Science and Engineering Center for Nanocarbons, Beijing National Laboratory for Molecular Sciences, College of Chemistry and Molecular Engineering, Peking University, Beijing 100871, PR China. <sup>5</sup>Beijing Graphene Institute, Beijing 100095, PR China. <sup>6</sup>Academy for Advanced Interdisciplinary Studies, College of Engineering, Peking University, Beijing 100871, PR China. <sup>7</sup>Department of Chemical Engineering and Analytical Science, University of Manchester, Manchester M13 9PL, UK. ✉email: [michele.merano@unipd.it](mailto:michele.merano@unipd.it)

One of the great achievements in materials science is certainly the isolation of individual crystal planes, starting from solids with strong in-plane bonds and weak, van der Waals-like, coupling between layers. In general, when dealing with layered crystals, Maxwell's equations increase in complexity in order to account for anisotropy. The susceptibility of these materials is no longer described by a constant, but by a tensor and, as regards the optical properties, they are at least uniaxial. Consequently, we expect that the optical spectra of single-layer, two-dimensional (2D) crystals also show out-of-plane anisotropy. In spite of the fact that experimental assessment of the out-of-plane anisotropy for the three-dimensional crystals is manageable, this is not the case for isolated monolayers<sup>1</sup>. As a result, fifteen years after the exfoliation of the first atomically thin crystal, the exact description of its optical response remains an active and debated area of research<sup>2-7</sup>.

There are currently two main models in use for the linear optical description of single-layer crystals, the first is a thin film model that can be either isotropic or anisotropic along the vertical direction<sup>1,5,7-10</sup>. Optical contrast measurements, used to detect single and multiple layers of a 2D crystal, are analyzed by choosing an isotropic thin film<sup>5,7,10</sup>. This is justified by the normal incidence configuration: the electric field is parallel to the crystal and the in-plane optical constants dominate the optical response. Surprisingly, the same model applies to spectroscopic ellipsometry, a very sensitive technique that works at any angle of incidence. If the first ellipsometric data for graphene were fitted using a uniaxial thin film model<sup>8</sup>, the subsequent analysis concluded that ellipsometry is only sensitive to the in-plane optical constants<sup>1</sup>. This is because the sensitivity to anisotropy is dependent on the path length through the film, which is extremely limited for a monolayer<sup>1</sup>. We are aware of only two papers that claim the experimental observations of the out-of-plane optical constants of single-layer transition metal dichalcogenides (TMDC) deposited on some substrate<sup>11,12</sup>. These experiments show structures in the out-of-plane spectra that ab-initio calculations exclude<sup>13</sup>, meaning that these measurements face the same experimental limitation that all the other face<sup>1,8,9,14,15</sup>.

In the second model, the monolayer is treated as a 2D surface current without any thickness. In this case, the system is intrinsically anisotropic with both null out-of-plane surface susceptibility ( $\chi_{\perp}$ ) and conductivity ( $\sigma_{\perp}$ )<sup>3,6,16-18</sup>. If on one side the use of two different models is a sign of a physical richness, on the other it poses new conundrums. The two approaches, starting from the measured ellipsometric parameters, provide different in-plane surface susceptibility ( $\chi_{\parallel}$ ) and conductivity ( $\sigma_{\parallel}$ )<sup>14</sup>. For  $\chi_{\parallel}$ , this difference is greater than the experimental error<sup>14</sup>. From a theoretical point of view, the choice of setting  $\chi_{\perp} = 0$  m and  $\sigma_{\perp} = 0 \Omega^{-1}$  in the surface current model is arbitrary, yet so is the use of an isotropic thin film model, when we expect the system to be highly anisotropic. Ab-initio many body calculation of the optical spectra of graphite, graphene and bilayer graphene report interesting differences in the simulated out-of-plane properties going from the bulk limit, down to a monolayer, but they exclude a null value<sup>19</sup>, this also holds for other 2D crystals like TMDC<sup>13,20</sup>.

One main experimental problem in the analysis of the optical response of a 2D crystal is the role of the substrate, which adds a background signal, hiding the small contribution that comes from the out-of-plane optical constants. We measure  $\chi_{\parallel}$ ,  $\sigma_{\parallel}$ ,  $\chi_{\perp}$ , and  $\sigma_{\perp}$  in a two-step experiment (Fig. 1a, b). First, we extract the ellipsometric data ( $\Psi_s$ ,  $\Delta_s$ ) from a single-layer 2D crystal deposited on a transparent dielectric substrate, namely polydimethylsiloxane (PDMS). Then, the same crystal is completely immersed in PDMS for a second ellipsometric measurement that provides a

new set of data ( $\Psi_b$ ,  $\Delta_b$ ). By inverting the fundamental equation of ellipsometry  $\tan \Psi e^{i\Delta} = r_p/r_s$ , where  $r_p$  and  $r_s$  are the Fresnel coefficients, it is possible to extract  $\chi_{\parallel}$ ,  $\sigma_{\parallel}$ ,  $\chi_{\perp}$ ,  $\sigma_{\perp}$  from  $\Psi_s$ ,  $\Delta_s$ ,  $\Psi_b$ ,  $\Delta_b$ .

## Results and discussion

**Theoretical models.** While the reflection coefficients for the anisotropic slab model are reported in ref. <sup>21</sup>, it is much more difficult to find in the literature a complete and correct generalization of the surface current model to include also the orthogonal polarization. We provide here the essential conceptual steps. The detailed calculations of the Fresnel coefficients are in the Methods section. The parallel  $\vec{P}_{\parallel}$  and perpendicular  $\vec{P}_{\perp}$  polarizations to the crystal plane induce two surface currents:  $\vec{J}_{\parallel}$  and  $\vec{J}_{\perp}$  respectively. The reflected field is the superposition of the reflected fields from these two currents. We thus solve two set of boundary conditions<sup>22</sup>, one for  $\vec{J}_{\parallel}$ :

$$\begin{aligned} \hat{k} \wedge (\vec{H}_2 - \vec{H}_1) &= \frac{\partial \vec{P}_{\parallel}}{\partial t} = \vec{J}_{\parallel} \\ \hat{k} \wedge (\vec{E}_2 - \vec{E}_1) &= 0 \end{aligned} \quad (1)$$

and one for  $\vec{J}_{\perp}$ :

$$\begin{aligned} \hat{k} \wedge (\vec{H}_2 - \vec{H}_1) &= 0 \\ \hat{k} \wedge (\vec{E}_2 - \vec{E}_1) &= -\frac{1}{\epsilon_0} \hat{k} \wedge \text{grad}(P_{\perp}) = \vec{J}_{\perp} \end{aligned} \quad (2)$$

These boundary conditions were proposed first for metasurfaces<sup>23</sup> and then for 2D crystals in refs. <sup>4,24</sup>, where a surface current model with non-null  $\chi_{\perp}$ , and  $\sigma_{\perp}$  was applied to nonlinear graphene optics. Here  $\hat{k}$ ,  $\hat{i}$  are the unitary vectors in the  $z$  and  $x$  direction (Fig. 1),  $\vec{H}$  is the magnetic field,  $\vec{E}$  the electric field,  $\epsilon_0$  the vacuum permittivity and the subscripts 1 and 2 refer to the media above and below the monolayer. The first set of boundary conditions are discussed in refs. <sup>3,16,17</sup>, for the surface current model with null  $\vec{P}_{\perp}$ . The second set has the following simple explanation<sup>22,23,25</sup>. In the radiation zone<sup>26</sup>, the electromagnetic field due to an oscillating electric dipole in the  $\hat{k}$ , direction is identical to an electromagnetic field due to an oscillating magnetic dipole in the  $-\hat{i}$  direction. This last one would cause a jump in the tangential component of  $\vec{E}$ .

Assuming a time dependence  $e^{i\omega t}$ , ( $\omega$  is the angular frequency of the light) for a monolayer completely immersed in a dielectric medium of refractive index  $n$  we find:

$$r_{ip} = \frac{(ik\chi_{\parallel} + \sigma_{\parallel}\eta) \cos \theta}{(ik\chi_{\parallel} + \sigma_{\parallel}\eta) \cos \theta + 2n} - \frac{n(ik\chi_{\perp} + \sigma_{\perp}\eta) \tan \theta \sin \theta}{2 + n(ik\chi_{\perp} + \sigma_{\perp}\eta) \tan \theta \sin \theta} \quad (3)$$

where the subscript  $i$  denotes that the sample is immersed,  $p$  is in place of  $p$ -polarized light,  $k$  is the wave vector of light in vacuum,  $\eta$  is the impedance of vacuum and  $\theta$  is the angle of incidence. For a monolayer deposited at the interface of vacuum with a dielectric substrate of refractive index  $n$  we find:

$$\begin{aligned} r_{sp} = & -\frac{n \cos \theta - \cos \theta_t}{n \cos \theta + \cos \theta_t} + \frac{n \cos \theta - \cos \theta_t + (ik\chi_{\parallel} + \sigma_{\parallel}\eta) \cos \theta \cos \theta_t}{n \cos \theta + \cos \theta_t + (ik\chi_{\parallel} + \sigma_{\parallel}\eta) \cos \theta \cos \theta_t} \\ & + \frac{n^2 \cos \theta - n \cos \theta_t - (ik\chi_{\perp} + \sigma_{\perp}\eta) \sin^2 \theta}{n^2 \cos \theta + n \cos \theta_t + (ik\chi_{\perp} + \sigma_{\perp}\eta) \sin^2 \theta} \end{aligned} \quad (4)$$

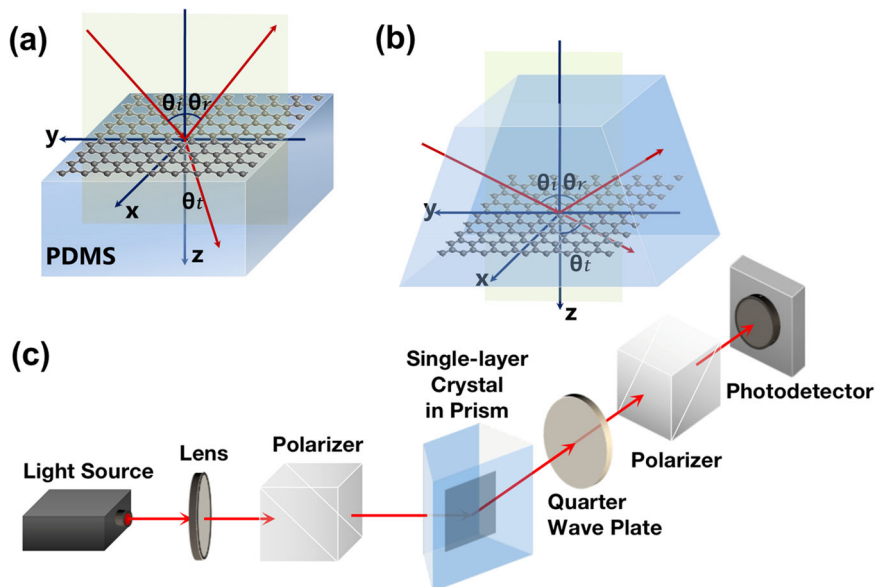


**Fig. 1 Experimental set up.** **a** First step of the experiment: standard spectroscopic ellipsometry on a single-layer 2D crystal deposited on a polydimethylsiloxane (PDMS) substrate. **b** Second step of the experiment: manual ellipsometric measurement on the same crystal completely immersed in a PDMS prism. **c** Set up of the manual ellipsometer, at the wavelength of 633 nm.

where the subscript  $s$  denotes the substrate, and  $\theta_i$  is the propagation angle in the dielectric. For  $s$  polarized light the Fresnel coefficients depend only on  $\chi_{\parallel}$ ,  $\sigma_{\parallel}$  and are provided in formula (6) of ref. <sup>3</sup>.

**Experimental procedure.** In our experiment, a  $7 \times 7$  mm-size, polycrystalline, single-layer 2D crystal is deposited on a 1 cm thick (to avoid back reflections) PDMS substrate ( $2 \times 2$  cm square) by chemical vapor deposition (Fig. 1a). The first ellipsometric measurement (VASE ellipsometer, J. A. Woollam) provides  $\Psi_s$  and  $\Delta_s$  and the confirmation that we are dealing with a monolayer. We then place our sample in a prism-shaped mold (base  $6 \times 5$  cm, height 3.5 cm), we pour non-polymerized PDMS on it and we wait for complete polymerization. This process successfully produces a 2D crystal immersed in PDMS without any additional interface in between the previous and the newly added material. The prism has two optical quality lateral windows (Fig. 1b). The light reflected by the sample in this second step is 2 orders of magnitude less than in the previous one, because there is no more the substrate contribution. For this reason, we set up a manual ellipsometer at the wavelength of 633 nm (Fig. 1c) to measure  $\Psi_i$  and  $\Delta_i$ .

We studied both monolayer graphene and MoS<sub>2</sub>. First, we tested our two steps procedure without deposition of the monolayer to ensure that we do not observe any reflection in between the embedded substrate and the final prism. Ellipsometric parameters  $\Psi_s$  and  $\Delta_s$  are measured at angles of incidence  $\theta_s$  equal to 65° and 70° (Supplementary Figs. 1 and 2),  $\Psi_i$  and  $\Delta_i$  (Figs. 2a, b and 3 a, b) are taken at angles of incidence  $\theta_i$  around the pseudo-Brewster angle, where  $\Delta_i$  varies appreciably and  $\Psi_i$  has a minimum. When  $\theta_i$  becomes too small,  $\Delta_i$  approaches 180° and noise becomes dominant.

**Experimental data and comparison with different theoretical models.** Figures 2c, d, and 3c, d report the optical constants  $\chi_{\parallel}$ ,  $\sigma_{\parallel}$ ,  $\chi_{\perp}$ ,  $\sigma_{\perp}$  extracted from the ellipsometric data using the Fresnel coefficients provided by the anisotropic slab model (slab model) and by the surface current model (curr model). With no loss of information, for each  $\theta_i$  we report the average  $\chi_{\parallel}$ ,  $\sigma_{\parallel}$ ,  $\chi_{\perp}$ ,  $\sigma_{\perp}$  considering the  $\Psi_s$ ,  $\Delta_s$  at 65° and 70°. The curr model gives a positive  $\chi_{\perp}$  while the slab model a negative one. Within our present

experimental precision, we are not able to discriminate  $\sigma_{\perp}$  from zero. Both models provide similar  $\chi_{\parallel}$  and  $\sigma_{\parallel}$ .

It is possible to discriminate between the curr model and the slab model thanks to ab initio calculations that predict a positive  $\chi_{\perp}$ <sup>13</sup>. Reference<sup>19</sup> computes only  $\sigma_{\perp}$ , but Kramers–Kronig relations exclude a negative  $\chi_{\perp}$  in the visible spectrum even in this case. We also performed first-principles calculations explicitly focused on the visible domain (Supplementary Figs. 3 and 4). By considering the available theoretical predictions and the experimental data collected here, the surface current model seems the only one able to fit the data in good agreement with the computed optical constants.

As explained above, ellipsometric experiments are usually performed on samples deposited on a substrate. In this case, being only sensitive to the in-plane optical constants,  $\chi_{\parallel}$  and  $\sigma_{\parallel}$  are extracted using the isotropic slab model (iso\_slab model)<sup>1,8,9,15</sup> or the surface current model with null  $\chi_{\perp}$  and  $\sigma_{\perp}$  (curr\_0 model)<sup>14,16,17</sup>. Starting from the  $\Psi_s$  and  $\Delta_s$  (Supplementary Figs. 1 and 2), here we repeat this procedure to clarify its limits. The iso\_slab model provides  $\chi_{\parallel}$  and  $\sigma_{\parallel}$  that still agree with those obtained in our two-step experiment, while for the curr\_0 model only  $\sigma_{\parallel}$  looks acceptable. Table 1 resumes our results. Figures 2a, b, and 3a, b show that the iso\_slab model and the curr\_0 model are unable to fit the  $\Psi_i$  and  $\Delta_i$ . As expected these models are unable to account for the vertical anisotropy, once this is experimentally accessible.

We also measure the reflectivities  $R_{is} = |r_{is}^2|$  and  $R_{ip} = |r_{ip}^2|$ , for the sample immersed in PDMS (Figs. 2e, 3e). The observed values for  $R_{is}$  confirm the reliability of our experimental procedure because, being insensitive to  $\chi_{\perp}$  and  $\sigma_{\perp}$ , they can already be predicted after the first step of our experiment. This is a strong confirmation that immersion in PDMS does not alter the 2D crystal properties. As expected, for graphene  $R_{is}$  is one order of magnitude smaller than for MoS<sub>2</sub>. For  $p$  polarization we observe a pseudo-Brewster angle  $\theta_{pB}$ . The existence and the value of  $\theta_{pB}$  are very important in assessing the vertical anisotropy of single-layer graphene and MoS<sub>2</sub> (Table 1). The iso\_slab model predicts a wrong  $\theta_{pB}$ , the curr\_0 model does not predict it at all.

The study of a 2D crystal deposited on a substrate or immersed in a host material is by far the most common situation in the

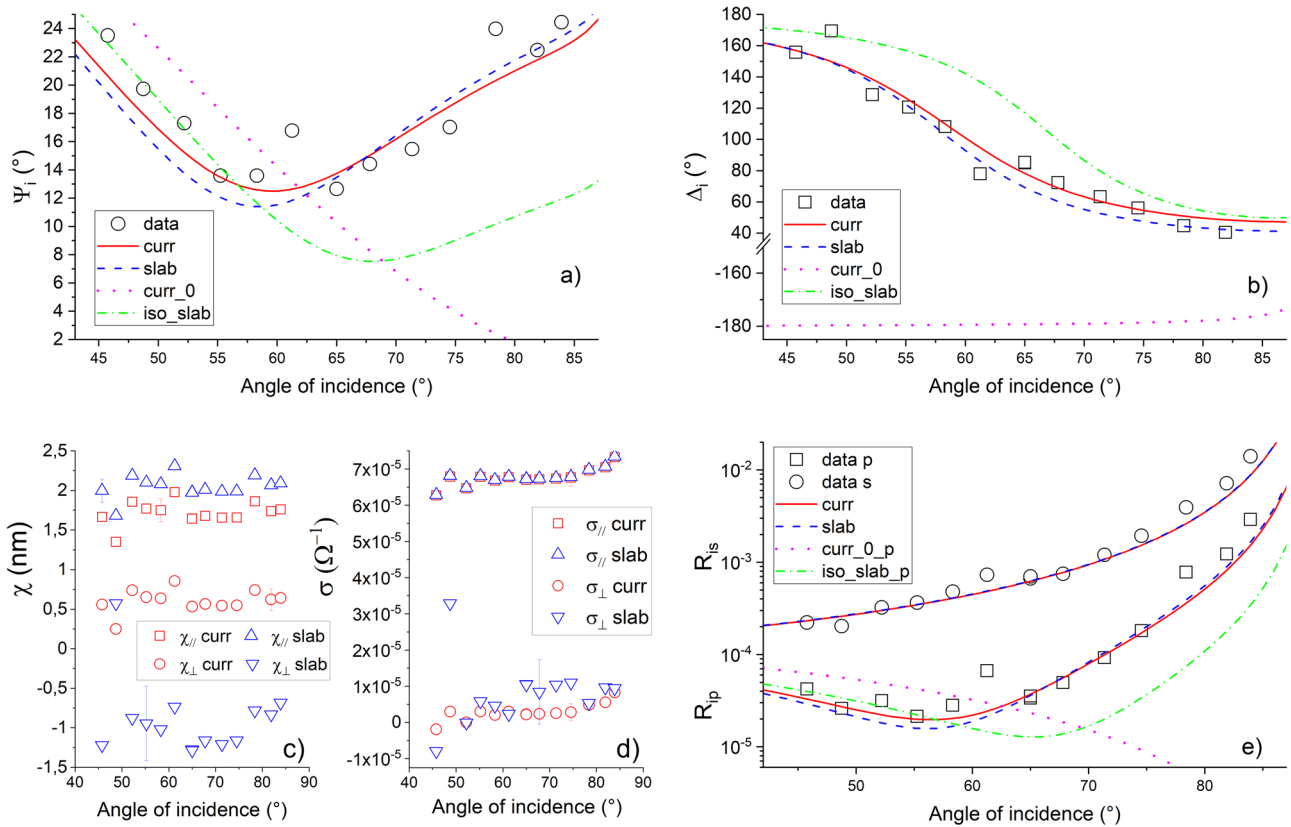


**Fig. 2 Experimental results for monolayer graphene immersed in polydimethylsiloxane.** Black dots: experimental data, colored dots: extracted optical constants, lines: theoretical fits for the four theoretical models considered in this paper. **a, b** Ellipsometric parameters  $\Psi_1$  and  $\Delta_1$ . Neither the iso\_slab model nor the curr\_0 model fit the data, using as optical constants those extracted from the  $\Psi_s$  and  $\Delta_s$ . **c, d** Optical constants determined with slab and the curr model. They predict similar  $\chi_{||}$  and  $\sigma_{||}$ , but negative and positive  $\chi_{\perp}$  respectively, and  $\sigma_{\perp}$  compatible with  $0 \Omega^{-1}$ . The error bars reported are the standard deviation of these values (see Table 1). **e** Reflectivities for s and p polarized light. Experimental data show a pseudo Brewster angle for  $R_{ip}$ . The iso\_slab model fails to predict its position by almost  $10^\circ$ . The curr\_0 model does not predict it at all. All models fit  $R_{is}$  reasonably well (for clarity we show only the curr model and the slab model).

laboratory. Still, measuring a free-standing monolayer<sup>27</sup> will be of great interest. If macroscopically this simply means a 2D crystal immersed in a medium with  $n = 1$  rather than 1.4233, microscopically it addresses the question on how much the host material affects the value of  $\chi_{\perp}$ . Our experimental results indicate that the influence of the host material is small. It remains to see if it is experimentally appreciable or not.

**Conclusions**

We have observed the role of  $\vec{P}_{\perp}$  in a single-layer 2D crystal, showing that it affects dramatically the position of  $\theta_{pB}$ . Our results state that  $\chi_{\perp}$  is a measurable optical constant way different from  $\chi_{||}$  or zero. These findings will have a deep impact in 2D crystal optics, opening new perspectives for fundamental science and technical developments. Based on present knowledge, we identify a single theoretical description<sup>22</sup> for a 2D crystal. Contrarily to what sometimes believed<sup>22</sup>, the slab and the surface current models are not equivalent even when we take  $\vec{P}_{\perp}$  into account. Out-of-plane anisotropy in 2D materials should play a role also in nonlinear optics<sup>28</sup>, surface wave phenomena<sup>29</sup> or magneto-optical Kerr effect<sup>30</sup> and any other field of 2D crystal optics. In view of the advances in photonics and optoelectronics of 2D semiconductors<sup>31,32</sup>, we expect a precise characterization of  $\chi_{\perp}$  and  $\sigma_{\perp}$  to become of great importance. A relevant open question is to what extent these quantities can be tuned in heterostructures for new functionalities<sup>33</sup>.

**Methods**

**Fresnel coefficients for the curr model (p-polarization)**

Insulator single-layer 2D crystal immersed in a dielectric medium of refractive index  $n$ . The electromagnetic fields satisfy:  $\frac{\partial}{\partial z} \vec{H} = \hat{s} \wedge \vec{E}$ ,  $\hat{s}$  being the unit vector along the propagation direction. We compute the reflected field due to  $\vec{j}_{||}$  by solving the boundary Eq. (1). In this case, the electric field parallel to the crystal plane is continuous across the crystal itself giving:

$$\vec{P}_{||} = \epsilon_0 \chi_{||} \vec{E}_{||}. \tag{5}$$

Choosing  $\vec{H}$  along  $-\hat{i}$ , Eq. (1) plus (5) run:

$$\begin{aligned} H_i + H_{r1} - H_{t1} &= \frac{ik}{\eta \epsilon_0} P_{||} \\ H_i - H_{r1} &= H_{t1} \\ H_{t1} &= \frac{n P_{||}}{\eta \epsilon_0 \chi_{||} \cos \theta} \end{aligned}$$

where the subscripts  $i, r, t$  denote the incident, reflected and transmitted fields. We compute the reflected field due to  $\vec{j}_{\perp}$  by solving the boundary Eq. (2). In this case, the electric field orthogonal to the crystal plane is continuous across the crystal itself giving:

$$\vec{P}_{\perp} = \epsilon_0 \chi_{\perp} \vec{E}_{\perp}. \tag{6}$$

Choosing  $\vec{H}$  along  $-\hat{i}$ , Eq. (2) plus (6) run:

$$\begin{aligned} H_i + H_{r2} &= H_{t2} \\ H_i - H_{r2} - H_{t2} &= \frac{ikn^2 P_{\perp} \tan \theta}{\eta \epsilon_0} \\ H_{t2} &= \frac{n P_{\perp}}{\eta \epsilon_0 \chi_{\perp} \sin \theta} \end{aligned}$$

In accordance to the superposition principle, the total reflected field is:  $H_r = H_{r1} + H_{r2}$ , the total transmitted field is:  $H_t = H_{t1} + H_{t2} - H_i = H_i - H_{r1} + H_{r2}$ .

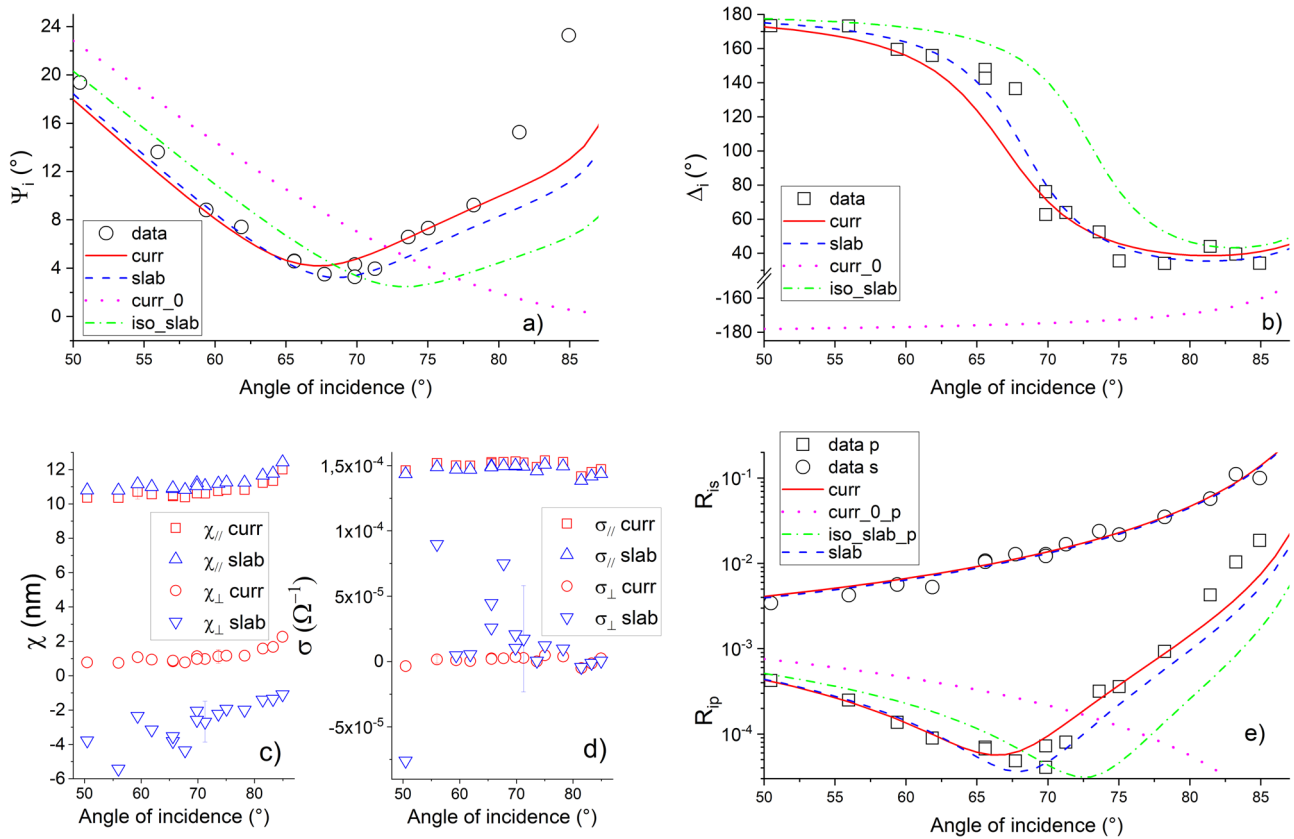


**Fig. 3 Experimental results for monolayer MoS<sub>2</sub> immersed in polydimethylsiloxane.** Black dots: experimental data, colored dots: extracted optical constants, lines: theoretical fits for the four models considered in this paper. **a, b** Ellipsometric parameters  $\Psi_i$  and  $\Delta_i$ . Neither the iso\_slab model nor the curr\_0 model fits the data, using as optical constants those extracted from the  $\Psi_s$  and  $\Delta_s$ . **c, d** Optical constants determined with slab and the curr model. They predict similar  $\chi_{\parallel}$  and  $\sigma_{\parallel}$ , but negative and positive  $\chi_{\perp}$  respectively, and  $\sigma_{\perp}$  compatible with  $0 \Omega^{-1}$ . The error bars reported are the standard deviation of these values (see Table 1). **e** Reflectivities for s and p polarized light. Experimental data show a pseudo Brewster angle for  $R_{ip}$ . The iso\_slab model fails to predict its position by almost 7°. The curr\_0 model does not predict it at all. All models fit  $R_{is}$  reasonably well (for clarity we show only the curr model and the slab model).

**Table 1 Optical constants for monolayer graphene and MoS<sub>2</sub>.**

Monolayer	Model	$\chi_{\parallel}$ (nm)	$\sigma_{\parallel}$ ( $10^{-5} \Omega^{-1}$ )	$\chi_{\perp}$ (nm)	$\sigma_{\perp}$ ( $10^{-6} \Omega^{-1}$ )	$\theta_{PB}$
Graphene	curr	$1.7 \pm 0.2$	$6.8 \pm 0.3$	$0.6 \pm 0.2$	$3 \pm 3$	$56.5^\circ$
	slab	$2.1 \pm 0.2$	$6.8 \pm 0.6$	$-0.9 \pm 0.5$	$9 \pm 9$	$56.3^\circ$
	iso_slab	$1.8 \pm 0.2$	$6.8 \pm 0.4$	$1.8 \pm 0.2$	$68 \pm 4$	$65.3^\circ$
	curr_0	$1.3 \pm 0.2$	$6.8 \pm 0.4$	0	0	No
MoS <sub>2</sub>	curr	$10.8 \pm 0.5$	$15.0 \pm 0.4$	$1.1 \pm 0.4$	$1 \pm 3$	$66.4^\circ$
	slab	$11.2 \pm 0.8$	$14.7 \pm 0.4$	$-2.7 \pm 1.2$	$14 \pm 41$	$67.9^\circ$
	iso_slab	$11.4 \pm 0.5$	$15.7 \pm 0.4$	$11.4 \pm 0.5$	$157 \pm 4$	$73.0^\circ$
	curr_0	$10.1 \pm 0.5$	$15.7 \pm 0.4$	0	0	No

For the curr and the slab models we report the average of the  $\chi_{\parallel}$ ,  $\sigma_{\parallel}$ ,  $\chi_{\perp}$ ,  $\sigma_{\perp}$  extracted from the  $\Psi_s$ ,  $\Delta_s$ ,  $\Psi_i$ ,  $\Delta_i$ . The error in this case is the standard deviation of these values. For the iso-slab and the curr\_0 model we report the  $\chi_{\parallel}$ ,  $\sigma_{\parallel}$  ( $\chi_{\perp}$ ,  $\sigma_{\perp}$  being trivially fixed) extracted from the  $\Psi_s$ ,  $\Delta_s$ .  $\theta_{PB}$ : pseudo-Brewster angle expected for the different models.

The reflection and the transmission coefficients are respectively:  $r_{ip} = \frac{H_i}{H_i}$ ;  $t_{ip} = \frac{H_i}{H_i}$ .

We verify that:  $R_{ip} + T_{ip} = 1$ , where  $T_{ip} = |t_{ip}^2|$ .

Insulator single-layer 2D crystal at the vacuum-dielectric medium interface. The electromagnetic fields in vacuum satisfy:  $\eta \vec{H} = \hat{s} \wedge \vec{E}$ . For  $\vec{J}_{\parallel}$  Eq. (1) plus (5) run:

$$\begin{aligned}
 H_i + H_{r1} - H_{t1} &= \frac{ik}{\eta \epsilon_0} P_{\parallel} \\
 (H_i - H_{r1}) \cos \theta &= \frac{H_{t1} \cos \theta_t}{n} \\
 H_{t1} &= \frac{n P_{\parallel}}{\eta \epsilon_0 \chi_{\parallel} \cos \theta_t}
 \end{aligned}$$

For  $\vec{J}_{\perp}$  Eq. (2) plus (6) run:

$$\begin{aligned}
 H_i + H_{r2} &= H_{t2} \\
 (H_i - H_{r2}) \cos \theta &= \frac{H_{t2} \cos \theta_t}{n} = \frac{ik P_{\perp} \sin \theta}{\eta \epsilon_0} \\
 H_{t2} &= \frac{n^2 P_{\perp}}{\eta \epsilon_0 \chi_{\perp} \sin \theta}
 \end{aligned}$$

In accordance to the superposition principle, the total reflected field is:  $H_r = H_{r1} + H_{r2} - H_{rp}$ , the total transmitted field is:  $H_t = H_{t1} + H_{t2} - H_{tp}$ , where  $H_{rn}$  and  $H_{tn}$  are the fields reflected and transmitted without the 2D crystal deposited at the interface. The Fresnel coefficients are defined as above, and from energy flux considerations:  $R_{ip} + \frac{n \cos \theta_t}{\cos \theta} T_{ip} = 1$ . Thanks to the application of the superposition

principle, our connection of  $\vec{P}_{\parallel}$  and  $\vec{P}_{\perp}$  with the macroscopic field is straightforward. This principle is not usually applied in the literature<sup>4,23,24</sup> forcing to definitions different from (5) and (6). Unfortunately, this last approach does not seem to verify energy flux conservation that we expect valid for insulators.

For conducting 2D crystals we have to modify the definition of  $\vec{J}_{\parallel}$  in (1):

$$\vec{J}_{\parallel} = \frac{\partial \vec{P}_{\parallel}}{\partial t} + \vec{J}_{\sigma_{\parallel}}, \text{ where:}$$

$$\vec{J}_{\sigma_{\parallel}} = \sigma_{\parallel} \vec{E}_{\parallel} \quad (7)$$

and the definition of  $\vec{J}_{\perp}$  in (2)<sup>25</sup>:  $\vec{J}_{\perp} = -\frac{1}{\epsilon_0} \hat{k} \wedge \text{grad} \left( P_{\perp} + \frac{I_{\perp}^{\perp}}{\omega} \right)$  where:

$$\vec{J}_{\sigma_{\perp}} = \sigma_{\perp} \vec{E}_{\perp}. \quad (8)$$

We then compute the reflected and the transmitted fields due to  $\vec{J}_{\parallel}$  by solving Eqs. (1), (5), and (7) and those due to  $\vec{J}_{\perp}$  by solving Eqs. (2), (6), and (8).

### Sample preparation

**Monolayer graphene growth and transfer.** We have prepared one large-area (up to mm), polycrystalline, continuous, single-layer graphene with chemical vapor deposition (CVD). Monolayer graphene grows on commercial Cu foils (50  $\mu\text{m}$  thick, Kunshan luzhifa Electronic Technology Co., Ltd) via a low-pressure CVD system. Cu foil is annealed at 1020  $^{\circ}\text{C}$  under a 500 sccm flow of Ar with a 0.1 sccm flow of  $\text{O}_2$  (0.1% of diluted  $\text{O}_2$  in Ar) for 30 min. Then, graphene grows under 500 sccm flow of  $\text{H}_2$  and a step increased flow rate of  $\text{CH}_4$  (0.5 sccm for 20 min, 0.8 sccm for 20 min, and then 1.2 sccm for 40 min)<sup>34</sup>. For the graphene transfer, poly(methyl-methacrylate) (PMMA) is spin-coated on as-grown graphene on Cu at 2000 rpm and baked at 170  $^{\circ}\text{C}$  for 3 min. The Cu foil is then etched away by  $\text{Na}_2\text{S}_2\text{O}_8$  (1 mol/L) after the graphene on the other side of Cu (graphene was grown on both sides of Cu foils) is removed by air plasma (10 sccm and power of 100 W). Subsequently, the freestanding PMMA/graphene stack floating on  $\text{Na}_2\text{S}_2\text{O}_8$  solution is washed with deionized water for four times, and salvaged by the PDMS, forming the PMMA/graphene/PDMS structure. After the as-formed PMMA/graphene/PDMS is dried, the PMMA is removed by immersion in acetone at 80  $^{\circ}\text{C}$  for 10 min and it forms the graphene/PDMS structure.

**Monolayer  $\text{MoS}_2$  growth and transfer.** We have prepared one large-area (up to mm), polycrystalline, continuous, single-layer  $\text{MoS}_2$  with CVD. Monolayer  $\text{MoS}_2$  grows on soda-lime glass using a three-zone tube furnace under a low-pressure atmosphere. A piece of Mo foil (Alfa Aesar, 9.95%; 0.025 mm thick) was folded as a “bridge” and placed on top of the glass substrate with a gap of 10 mm. S power (Alfa Aesar, purity 99.5%) was located at upstream of the furnace. Before heating, the system was purged with Ar (80 sccm) for 10 min to get out of the air. Then, Ar (50 sccm) and  $\text{O}_2$  (6 sccm) mixed gas flows were introduced into the system to create a stable growth atmosphere. The temperature of the S powder and the glass substrate was set at 100  $^{\circ}\text{C}$  and 720  $^{\circ}\text{C}$ , respectively. The growth time was set at 1–3 min. After growth, the furnace was naturally cooled to room temperature. The as-synthesized  $\text{MoS}_2$  monolayer/soda-lime samples were firstly spin-coated with PMMA at 1000 rpm for 1 min, followed by baking at 80  $^{\circ}\text{C}$  for 20 min. The PMMA-supported samples were then inclined into the pure water, and the PMMA/ $\text{MoS}_2$  complex was naturally peeled off under the surface tension effect. The PMMA/ $\text{MoS}_2$  film was collected by PDMS. Finally, the PMMA film was removed via acetone.

**Role of sample doping.** It is well known that the transfer process would inevitably induce p-doping in the graphene<sup>35,36</sup>. As for  $\text{MoS}_2$ , n-doping is usually obtained due to S-vacancy. Fortunately, in our experiments, the optical performance agrees well with previous measurements for in-plane optical constants and with ab-initio theoretical predictions. So, we believe that our conclusion is robust, regardless of the doping level or doping type.

**PDMS substrate preparation and immersion of the 2D crystal in PDMS.** The PDMS (Sylgard 184, by Dow Corning) substrate is prepared by mixing the base elastomer and the curing agent in ratio 10:1, and by 72 h room temperature (RT) polymerization. Then, after the deposition of the monolayer 2D crystal (see above), new pre-polymerized PDMS is poured on the structure, using a 3D printed prism shape structure (ABS filament) as mold. We again wait for RT polymerization. Since the 3D printed structure presents a high roughness that would compromise the optical measurements, glass slides are glued on them. In this way, we obtain a PDMS prism with optical quality lateral windows. To prevent the PDMS bonding to the glass slides during the polymerization process, a fluorinated antiadhesive coating (Trichloro(1H,1H,2H,2H-perfluorooctyl) silane, by Sigma-Aldrich) is applied.

Some strain effects could be there on 2D materials during the PMDS polymerization process. These are difficult to estimate but we find the same in-plane optical constants before and after immersion. For this reason, strain, if present, is not supposed to alter our conclusions. We can also wonder how much the dielectric screening of PDMS can influence the measured optical constants before and after immersion in it (especially for  $\text{MoS}_2$ ). Reference<sup>37</sup> shows that these effects are large only when capping with materials having a large dielectric constant

(see. Figure 3 of ref. <sup>37</sup>). The PDMS dielectric constant is 1.96, and this is the reason why we do not observe a variation of the optical response.

### Measurement and determination of the optical constants

**Spectroscopic ellipsometry of a 2D crystal deposited on a PDMS substrate.** Spectroscopic ellipsometric measurements are performed using a VASE ellipsometer (J. A. Wollam) in ambient conditions at room temperature. We follow the same procedure described in<sup>14</sup>. The first step of our analysis is the characterization of the substrate. The ellipsometric  $\Psi$  parameter of the substrate alone is perfectly fitted by assuming a refractive index  $n$  given by the Sellmeier expression<sup>38</sup> minus a constant value of 0.005. At a wavelength of 633 nm we have  $n = 1.4233$ . For graphene, the use of this measured value instead of the one reported in the literature<sup>38</sup> is responsible for a difference of 0.06 nm,  $1 \cdot 10^{-6} \Omega^{-1}$ , 0.06 nm and  $9 \cdot 10^{-6} \Omega^{-1}$  respectively for  $\chi_{\perp}$ ,  $\sigma_{\perp}$ ,  $\chi_{\parallel}$ , and  $\sigma_{\parallel}$ . Only the discrepancy for  $\sigma_{\parallel}$  is bigger than the error in the measurements (Table 1). Although small, this last difference shows the importance of a careful substrate characterization when dealing with monolayers. For  $\text{MoS}_2$  these discrepancies are even smaller than for graphene and equal respectively to 0.02 nm,  $7 \cdot 10^{-7} \Omega^{-1}$ , 0.03 nm and  $9 \cdot 10^{-6} \Omega^{-1}$ .

Supplementary Figures 1 and 2 show the ellipsometric parameter  $\Psi_s$  and  $\Delta_s$  of single-layer graphene and  $\text{MoS}_2$  deposited on a PDMS substrate. Starting from these data, ref. <sup>14</sup> describes how we extract  $\chi_{\parallel}$  and  $\sigma_{\parallel}$  for the iso\_slab model and the curr\_0 model.

**Manual ellipsometer.** The light source is a HeNe laser at a wavelength of 633 nm. A lens (focal length 40 cm) focuses the Gaussian beam to a  $1/e^2$  intensity diameter of 120  $\mu\text{m}$  allowing measurements at grazing incidence. We set the first polarizer at an azimuthal angle of 45 $^{\circ}$ . The light intensity after the first polarizer is typically 4 mW. A quarter wave plate (QWP) and a second polarizer (the analyzer) perform ellipsometric measurements. We fully characterize the vibrational ellipse for the electric vector of the light reflected from the sample<sup>39</sup>. Without the QWP installed, we measure the  $s$  and  $p$  components of the reflected light. Then we identify the azimuthal angles of the minor and the major axes of the ellipse. Finally, we place the QWP with the fast axis along the minor axis. After this, the azimuthal angle of the analyzer, corresponding to a minimum power on the photodetector, fixes the sense in which the endpoint of the electric vector describes the ellipse (the sign of  $\Delta_i$ ). The power meter used in our measurements has a resolution of 1 nW. Only the 2D crystal introduces a phase difference ( $\Delta_i$ ) in between the  $s$  and  $p$  components of the incident linearly polarized light. Transmission through the two prism sides only introduces a different power reduction in  $s$  and  $p$ , important for the correct evaluation of  $\Psi_s$ ,  $R_{is}$ , and  $R_{ip}$ . The QWP is antireflection coated at 633 nm while the analyzer introduces an identical power reduction in  $s$  and  $p$  (important for a correct evaluation of  $R_{is}$  and  $R_{ip}$ ).

We are unable to estimate  $\sigma_{\perp}$  because it is much smaller (Supplementary Fig. 6) than our experimental error. We are limited by the quality of the reflected beam and by some scattering. The poor quality of the reflected beam is a consequence of the macroscopic quality of our 2D crystals. Even if we are dealing with some of the best samples available in the world, any small defect affects the reflection of a highly coherent laser source. A few amounts of unwanted scattering come from the back surface of the prism that is far from perfect because of handling or, for some angles of incidence, from the prism corners.

**First-principles calculations.** Layer susceptibilities have been evaluated using first-principles many-body perturbation theory calculations of periodic dielectric layers. First, density functional theory (DFT) orbitals were obtained with the so-called PBE exchange and correlation functional<sup>40</sup> at the theoretical lattice constant using the Quantum-Espresso DFT software package<sup>41</sup>. Then, the screened Coulomb interaction  $W$ <sup>42</sup> was found using the  $G_0W_0$  approach (GWL program<sup>43</sup>). The Brillouin zones were sampled at the sole  $\Gamma$  point albeit adopting supercells comprising 8 atoms for graphene and 12 atoms for  $\text{MoS}_2$ . An optimal polarizability basis of 800 vectors was applied for developing the polarizability operators. Finally, the in-plane  $\epsilon_{\parallel}$  and out-of-plane  $\epsilon_{\perp}$  components of the complex dielectric tensors relative to the periodic thin dielectric layers were calculated including electron-hole interactions using the Bethe-Salpeter equation scheme<sup>44,45</sup> (simple.x code<sup>46</sup>).

For graphene, we used a  $12 \times 12 \times 12$  regular mesh of k-points for sampling the Brillouin zone (relative to the super-cell) which was shifted in order not to contain the  $\Gamma$  point and we included 12 occupied and 48 unoccupied orbitals. A stretching factor of 1.67 was applied to the DFT valence and conduction bands in order to match GW energies in the proximity of the band closure at the  $K$ -point. These GW values were obtained extrapolating, to the bulk limit, results for models of 12 and 32 atoms.

For  $\text{MoS}_2$ , we used a  $6 \times 6 \times 6$  regular mesh of k-points for sampling the Brillouin zone (relative to the super-cell) together with a fully relativistic treatment of the spin-orbit coupling. We included 56 occupied and 96 unoccupied orbitals. A scissor factor of 1.30 eV was applied to the DFT band structure in order that the DFT gap matches the bulk limit of the GW one. The latter was evaluated at the scalar relativistic level. Moreover, for  $\text{MoS}_2$  we added a constant term of 2.13 to  $\epsilon_{\parallel}$  and one of 1.33 to  $\epsilon_{\perp}$  in order to account for the upper unoccupied orbitals which were not included in the BSE calculation. These factors were chosen in order to match the corresponding components of the dielectric tensor calculated from density functional perturbation theory.

It is worth noting that the calculated BSE susceptibilities exhibit only a mild dependence on the strategy chosen for updating the DFT bands in order to account for GW effects. In particular, the out-of-plane responses are particularly insensitive as it is shown, for MoS<sub>2</sub> in Supplementary Figs. 5 and 6 where we report results obtained using scissor factors of 1.0, 1.3 eV and a scissor factor of 1.0 accompanied by a stretching one of 1.2 for both manifolds as in ref. 47.

The in-plane  $\chi_{C\parallel}$  and out-of-plane  $\chi_{C\perp}$  complex susceptibilities are rigorously defined as the ratio between the induced surface dipole densities with respect to the transmitted electric field. In the case of  $\chi_{C\parallel}$  the transmitted field is parallel to the 2D layer and is conserved along the simulation cell. It is worth noting<sup>43</sup> that in first-principles simulations with periodic boundary conditions (PBC) the directly accessible quantity is the response with respect to the total or internal (electric) field. This is due to incommensurate extension of the field with respect to the length period of the PBC. This makes it possible to obtain  $\chi_{C\parallel}$  from  $\epsilon_{\parallel}$ :

$$\chi_{C\parallel} = L(\epsilon_{\parallel} - 1) \quad (9)$$

where  $L$  is the periodic length of the simulation cell in the direction perpendicular to the 2D layer. This length is big from a microscopic point of view in order to null the interaction between the atomic layers but small from a macroscopic point of view (for instance it is much smaller than the wavelength of the incident light).

For  $\chi_{C\perp}$  the transmitted electric field  $E_{t\perp}$ , which is now perpendicular to the 2D layer, can be found<sup>48</sup> from  $\epsilon_{\perp}$ :

$$E_{t\perp} = \frac{E_{cell}}{\epsilon_{\perp}} \quad (10)$$

where  $E_{cell}$  is the perpendicular long-range electric field accounted for in the calculation of  $\epsilon_{\perp}$ . Hence, the out-of-plane complex susceptibility is given by:

$$\chi_{C\perp} = \frac{L(\epsilon_{\perp} - 1)}{\epsilon_{\perp}} \quad (11)$$

Equations 1 and 3 have been reported previously<sup>13,22</sup>. Reference<sup>13</sup> derive them to model a dielectric layer as an infinitesimally thin sheet. Reference<sup>22</sup> derives them from the effects of local fields to the dielectric responses.

For evaluating  $\epsilon_{\parallel}$  and  $\epsilon_{\perp}$ , we applied first a Lorentzian broadening of 0.1 eV and then a Gaussian one of 0.2 eV<sup>19</sup>. The surface susceptibilities measured in this paper are the real part of  $\chi_{C\parallel}$  and  $\chi_{C\perp}$ , the surface conductivities are proportional to the imaginary part of  $\chi_{C\parallel}$  and  $\chi_{C\perp}$ <sup>9,14</sup>. Supplementary Figs. 3 and 4 report the computed out-of-plane optical constants in the visible spectrum. The in-plane optical constants are similar to those already reported in refs. 23,24,42.

## Data availability

Data sharing not applicable to this article as no datasets were generated or analyzed during the current study.

Received: 16 July 2021; Accepted: 11 August 2021;

Published online: 23 September 2021

## References

- Nelson, F. J. et al. Optical properties of large-area polycrystalline chemical vapor deposited graphene by spectroscopic ellipsometry. *Appl. Phys. Lett.* **97**, 253110 (2010).
- Li, Y. & Heinz, T. F. Two-dimensional models for the optical response of thin films. *2D Mater.* **5**, 025021 (2018).
- Merano, M. Fresnel coefficients of a two-dimensional atomic crystal. *Phys. Rev. A* **93**, 013832 (2016).
- Majérus, B., Dremetsika, E., Lobet, M., Henrard, L. & Kockaert, P. Electrodynamics of two-dimensional materials: role of anisotropy. *Phys. Rev. B* **98**, 125419 (2018).
- Bruna, M. & Borini, S. Optical constants of graphene layers in the visible range. *Appl. Phys. Lett.* **94**, 031901 (2009).
- Chang, Y.-C., Liu, C.-H., Liu, C.-H., Zhong, Z. & Norris, T. B. Extracting the complex optical conductivity of mono- and bilayer graphene by ellipsometry. *Appl. Phys. Lett.* **104**, 261909 (2014).
- Blake, P. et al. Making graphene visible. *Appl. Phys. Lett.* **91**, 063124 (2007).
- Kravets, V. G. et al. Spectroscopic ellipsometry of graphene and an exciton-shifted van Hove peak in absorption. *Phys. Rev. B* **81**, 155413 (2010).
- Li, Y. et al. Measurement of the optical dielectric function of monolayer transition-metal dichalcogenides: MoS<sub>2</sub>, MoSe<sub>2</sub>, WS<sub>2</sub>, and WSe<sub>2</sub>. *Phys. Rev. B* **90**, 125706 (2014).
- Benameur, M. M. et al. Visibility of dichalcogenide nanolayers. *Nanotechnology* **22**, 125706 (2011).
- Funke, S., Miller, B., Parzinger, E., Thiesen, P. & Wurstbauer, U. Imaging spectroscopic ellipsometry of MoS<sub>2</sub>. *J. Phys. Condens. Matter* **28**, 385301 (2016).
- Chu, Y. & Zhang, Z. Birefringent and complex dielectric functions of monolayer WSe<sub>2</sub> derived by spectroscopic ellipsometer. *J. Phys. Chem. C* **124**, 12665–12671 (2020).
- Guilhon, I. et al. Out-of-plane excitons in two-dimensional crystals. *Phys. Rev. B* **99**, 161201 (2019).
- Jayaswal, G. et al. Measurement of the surface susceptibility and the surface conductivity of atomically thin MoS<sub>2</sub> by spectroscopic ellipsometry. *Opt. Lett.* **43**, 703–706 (2018).
- Li, W. et al. Broadband optical properties of large-area monolayer CVD molybdenum disulfide. *Phys. Rev. B* **90**, 195434 (2014).
- Hanson, G. W. Dyadic Green's functions and guided surface waves for a surface conductivity model of graphene. *J. Appl. Phys.* **103**, 064302 (2008).
- Falkovsky, L. A. & Pershoguba, S. S. Optical far-infrared properties of a graphene monolayer and multilayer. *Phys. Rev. B* **76**, 153410 (2007).
- Zhan, T., Shi, X., Dai, Y., Liu, X. & Zi, J. Transfer matrix method for optics in graphene layers. *J. Phys. Condens. Matter* **25**, 215301 (2013).
- Trevisanutto, P. E., Holzmann, M., Coté, M. & Olevano, V. Ab initio high-energy excitonic effects in graphite and graphene. *Phys. Rev. B* **81**, 121405 (2010).
- Laturia, A., Van, D. & Vandenberghe, W. G. Dielectric properties of hexagonal boron nitride and transition metal dichalcogenides: from monolayer to bulk. *NPJ 2D Mater. Appl.* **2**, 1–6 (2018).
- Azzam, R. M. A. & Bashara, N. M. Ellipsometry and Polarized Light. 356–357 (North-Holland publishing company, Amsterdam, 1977).
- Senior, T. B. A. & Volakis, J. L. Sheet simulation of a thin dielectric layer. *Radio Sci.* **22**, 1261–1272 (1987).
- Kuester, E. F., Mohamed, M. A., Picket-May, M. & Holloway, C. L. Averaged transition conditions for electromagnetic fields at a metafilm. *IEEE Trans. Antennas Propag.* **51**, 2641–2651 (2003).
- Dremetsika, E. & Kockaert, P. Enhanced optical Kerr effect method for a detailed characterization of the third-order nonlinearity of two-dimensional materials applied to graphene. *Phys. Rev. B* **96**, 235422.235421–235422.235427 (2017).
- Idemen, M. Universal boundary relations of the electromagnetic field. *J. Phys. Soc. Jpn.* **59**, 71–80 (1990).
- Jackson, J. D. Classical Electrodynamics, 3rd ed., 413–414 (Wiley, New York, 1998).
- Nair, R. R. et al. Fine structure constant defines visual transparency of graphene. *Science* **320**, 1308 (2008).
- Kumar, N. et al. Second harmonic microscopy of monolayer MoS<sub>2</sub>. *Phys. Rev. B* **87**, 161403 (2013).
- Fei, Z. et al. Gate-tuning of graphene plasmons revealed by infrared nano-imaging. *Nature* **487**, 82–85 (2012).
- Huang, B. et al. Layer-dependent ferromagnetism in a van der Waals crystal down to the monolayer limit. *Nature* **546**, 270–273 (2017).
- Mak, K. F. & Shan, J. Photonics and optoelectronics of 2D semiconductor transition metal dichalcogenides. *Nat. Photonics* **10**, 216–226 (2016).
- Mak, K. F., Lee, C., Hone, J., Shan, J. & Heinz, T. F. Atomically thin MoS<sub>2</sub>: a new direct-gap semiconductor. *Phys. Rev. Lett.* **105**, 136805 (2010).
- Geim, A. K. & Grigorieva, I. V. Van der Waals heterostructures. *Nature* **499**, 419–425 (2013).
- Sun, L. et al. Visualizing fast growth of large single-crystalline graphene by tunable isotopic carbon source. *Nano Res.* **10**, 355–363 (2016).
- Chen, Y., Gong, X. L. & Gai, J. G. Progress and challenges in transfer of large-area graphene films. *Adv. Sci.* **3**, 1500343 (2016).
- Wu, Z. et al. Step-by-step monitoring of CVD-graphene during wet transfer by Raman spectroscopy. *RSC Adv.* **9**, 41447–41452 (2019).
- Raja, A. et al. Coulomb engineering of the bandgap and excitons in two-dimensional materials. *Nat. Commun.* **8**, 15251 (2017).
- Schneider, F., Draheim, J., Kamberger, R. & Wallrabe, U. Process and material properties of polydimethylsiloxane (PDMS) for optical MEMS. *Sens. Actuat. A: Phys.* **151**, 95–99 (2009).
- Born, M. & Wolf, E. Principles of Optics, 5th ed. (Pergamon Press, London, 1975).
- Perdew, J. P., Burke, K. & Ernzerhof, M. Generalized gradient approximation made simple. *Phys. Rev. Lett.* **77**, 3865–3868 (1996).
- Giannozzi, P. et al. Advanced capabilities for materials modelling with quantum ESPRESSO. *J. Phys. Condens. Matter* **29**, 465901 (2017).
- Hybertsen, M. S. & Louie, S. G. Electron correlation in semiconductors and insulators: Band gaps and quasiparticle energies. *Phys. Rev. B* **34**, 5390–5413 (1986).
- Umari, P., Stenuit, G. & Baroni, S. GW quasi-particle spectra from occupied states only. *Phys. Rev. B* **81**, 115104 (2009).
- Albrecht, S., Reining, L., Del Sole, R. & Onida, G. Ab initio calculation of excitonic effects in the optical spectra of semiconductors. *Phys. Rev. Lett.* **80**, 4510–4513 (1998).
- Rohlfing, M. & Louie, S. G. Electron-hole excitations in semiconductors and insulators. *Phys. Rev. Lett.* **81**, 2312–2315 (1998).

46. Prandini, G., Galante, M., Marzari, N. & Umari, P. SIMPLE code: optical properties with optimal basis functions. *Comput. Phys. Commun.* **240**, 106–119 (2019).
47. Elliott, J. D. et al. Surface susceptibility and conductivity of MoS<sub>2</sub> and WSe<sub>2</sub> monolayers: a first-principles and ellipsometry characterization. *Phys. Rev. B* **101**, 045414 (2020).
48. Stengel, M., Spaldin, N. A. & Vanderbilt, D. Electric displacement as the fundamental variable in electronic-structure calculations. *Nat. Phys.* **5**, 304–308 (2009).

### Acknowledgements

Z.X. and M.Me. acknowledge financial support from Dipartimento di Fisica e Astronomia G. Galilei, Università Degli Studi di Padova, funding BIRD170839/17. F.D. acknowledges STARS grant from Università Degli Studi di Padova.

### Author contributions

D.F. preparation of PDMS substrate and prism. L.S., Y.W., and Z.L. growth and transfer of graphene. P.Y. and Y.Z. growth and transfer of MoS<sub>2</sub>. Z.X., A.Z., N.G., A.M. and M.Me. optical measurements and data analysis. L.D.A. and M.Me. analytical theory. J.D.E. and P.U. ab-initio calculations for MoS<sub>2</sub>. M.Ma. and P.U. ab-initio calculations for graphene. M.Me. conceived the idea for the paper and drafted this manuscript. L.S., P.Y., M.Me., D.F., and P.U. wrote the section Methods. The manuscript was then read, improved and finally acknowledged by the other authors.

### Competing interests

The authors declare no competing interests.

### Additional information

**Supplementary information** The online version contains supplementary material available at <https://doi.org/10.1038/s42005-021-00711-3>.

**Correspondence** and requests for materials should be addressed to Michele Merano.

**Peer review information** *Communications Physics* thanks the anonymous reviewers for their contribution to the peer review of this work.

**Reprints and permission information** is available at <http://www.nature.com/reprints>

**Publisher's note** Springer Nature remains neutral with regard to jurisdictional claims in published maps and institutional affiliations.



**Open Access** This article is licensed under a Creative Commons Attribution 4.0 International License, which permits use, sharing, adaptation, distribution and reproduction in any medium or format, as long as you give appropriate credit to the original author(s) and the source, provide a link to the Creative Commons license, and indicate if changes were made. The images or other third party material in this article are included in the article's Creative Commons license, unless indicated otherwise in a credit line to the material. If material is not included in the article's Creative Commons license and your intended use is not permitted by statutory regulation or exceeds the permitted use, you will need to obtain permission directly from the copyright holder. To view a copy of this license, visit <http://creativecommons.org/licenses/by/4.0/>.

© The Author(s) 2021